

# TRANSIENT ANALYSES FOR THE MYRRHA-FASTEF REACTOR BY SIMMER CODE

**M. Angelucci, M. Eboli, N. Forgione**

Dipartimento di Ingegneria Civile e Industriale, Università di Pisa

Largo Lucio Lazzarino 2, 56126 Pisa, Italy

morena.angelucci@for.unipi.it; marica.eboli@for.unipi.it; nicola.forgione@ing.unipi.it

**G. Bandini**

ENEA - Centro Ricerche Ezio Clementel

Via Martiri di Monte Sole 4, 40129 Bologna, Italy

giacomino.bandini@enea.it

## ABSTRACT

This work illustrates 2D SIMMER-III and 3D SIMMER-IV calculations for fuel dispersion analyses during postulated accidents in the MYRRHA-FASTEF reactor. The aim was to identify some potential events which can involve a fuel release and the most affecting parameters for the recriticality concern.

In the first part, a 3D SIMMER-IV model of MYRRHA reactor is presented. It includes a gas region above the reactor that allows the simulation of transients in natural circulation flow. We found that the flow pattern which establishes in the primary circuit affects considerably the fuel dispersion phenomena. The low mass flow rate prevents the redistribution of the fuel that accumulates in the upper plenum. This model was used also to simulate two reference cases in forced circulation, showing no significant differences with respect to the analogous cases performed with the previous model, which did not include the gas region.

As 3D simulations required large CPU time, a SIMMER-III 2D model was likewise arranged for the long term analyses (up to 1-2 hours). The results highlighted some preferential accumulation points for the fuel particles in the long term. Nevertheless, in this case the influence of stagnation zones observed in 3D simulations cannot be adequately represented by SIMMER-III.

3D SIMMER-IV model was also used for the simulation of the Unprotected Loss of Flow Accident (ULOF) and the Unprotected Loss of Heat Sink (ULOHS) transients. The evolution of these transients did not show the likelihood of core degradation and release of fuel in the primary circuit within the time considered.

## KEYWORDS

**MYRRHA, SIMMER, fuel dispersion**

## 1 INTRODUCTION

Safety and reliability have considerable relevance in the design of nuclear reactors and are a key point for the public acceptance of the nuclear energy. These aspects are among the goals pursued in the development of the Generation IV nuclear reactors [1]. The recriticality risk after core disruptive accidents (CDAs) is one of the aspects to be taken into account in the frame of the safety analyses of Liquid Metal Fast Reactors. This aspect might be an issue if the fuel released from the core accumulates somewhere inside the primary circuit up to a critical configuration.

For Lead Cooled Reactors, the melting point of the stainless steel clad material (<1500°C) is lower than the boiling point of the coolant (1670°C). Therefore, clad melting and consequent fuel dislocation is expected before coolant boiling. The study of the fuel dispersion in case of releases from the core during a hypothetical severe accident is helpful for the identification of the most hazardous conditions for the

recriticality concern. In similar studies, Li et al. [2] analysed the core material redistribution processes with SIMMER-III code, for postulated flow blockage accidents. Further, 3D analyses on fuel dispersion for the MYRRHA reactor were also performed with CFD codes and results compared with SIMMER-IV ones [3].

In this work we performed several transients for the fuel dispersion analyses for the critical configuration of MYRRHA-FASTEF, with the aid of the SIMMER code. MYRRHA-FASTEF is the current design of the flexible experimental Accelerator-Driven System (ADS) under development at SCK-CEN, which can work in both subcritical and critical modes [4].

The code SIMMER-III was initially developed by JNC (now JAEA), CEA and FZK (now KIT), mainly for SFR safety studies [5]; extended at KIT for LFR. SIMMER-III is a two-dimensional multi-velocity-field, multi-phase, multi-component, Eulerian fluid-dynamics code coupled with a fuel-pin model and space- and energy-dependent neutron kinetics model. Nevertheless, the dimensionality is one of the major limitations of the code. Therefore, the development of SIMMER-IV, a three-dimensional code based on the SIMMER-III technology, was carried out by JAEA. It is the direct extension to three dimensions of SIMMER-III, without any changes in the physical models. The code framework is shown in Figure 1.1 [6]. For calculations described in the following, the neutronics part is not used, the power distribution and power variations vs. time being input data.

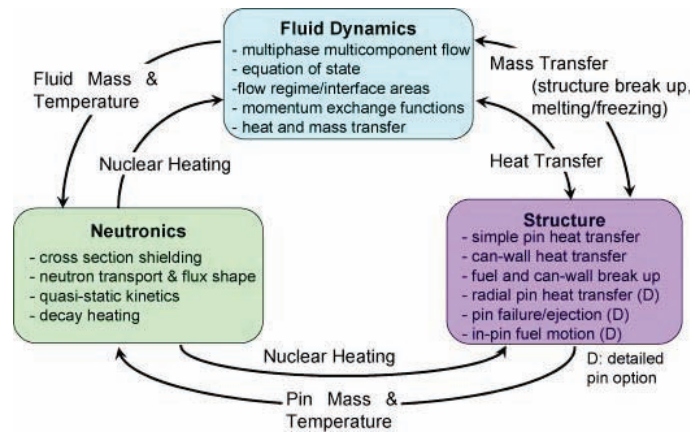


Figure 1.1: SIMMER-III Overall Code Structure.

## 2 SIMMER-IV MODEL OF MYRRHA-FASTEF REACTOR

A 3D model of MYRRHA reactor had been already written with the SIMMER-IV code in a previous work. It was realized in a Cartesian geometry through 65x63x42 cells and comprises the most important components, i.e. the vessel, the diaphragm, the 4 primary heat exchangers, the 2 primary pumps, the 2 in-vessel fuel handling machines (IVFHMs) and the core [7]. In the previous 3D model the cover gas region above the LBE region was removed due to convergence problems and extremely long computational time. Nevertheless, the cover gas region was necessary to simulate properly the coolant levels in the reactor during transients with transition to natural circulation. For this reason, a new 3D model with the cover gas region was set up. The internal components are represented with the same configuration and position of the previous model and a gas zone filled with Argon is set above the reactor. The new model has 50 cells along the axial direction.

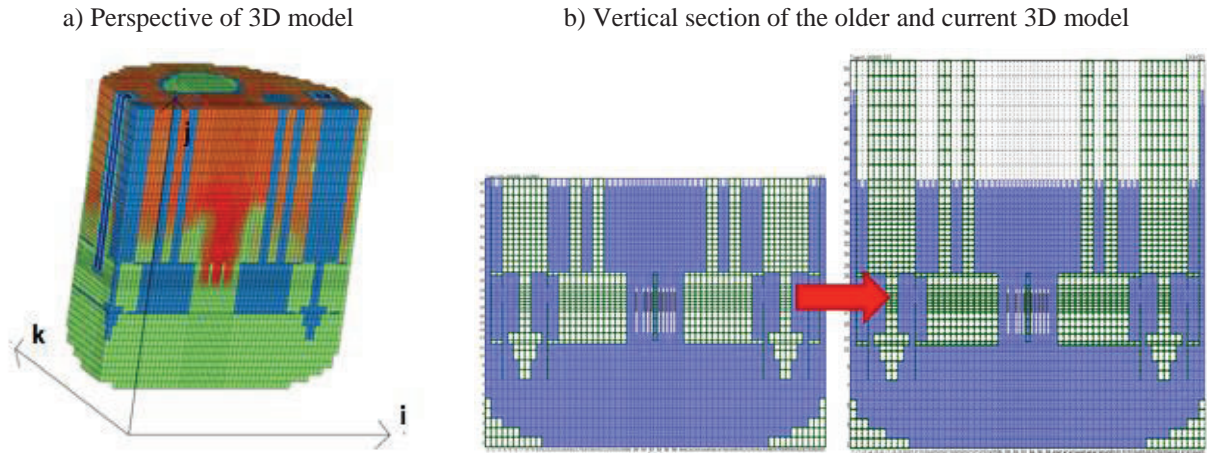


Figure 2.1: SIMMER-IV model of the MYRRHA FASTEF reactor.

## 2.1 Steady-State calculation

A steady-state computation was carried out to assess the suitability of the model. The configuration achieved is also used as starting point for the development of the transients. Due to long computational time, a simulation of 110 s is considered for the updated model ( $j=50$ ), even if a longer computation would have been preferable. In spite of this, some temperature and mass flow rate trends were checked to verify that the steady-state condition was reached. As reported in Figure 2.2, considered parameters tend to stabilize after 30 seconds. LBE temperature in the upper plenum seems not to be settled yet, maybe due to the temperature stratification that occurs at the core outlet. This phenomenon is linked to the presence of the external dummy assemblies that do not participate in power generation and also to the design and so to the modeling of the barrel holes. It should be mentioned that, in this model, the barrel holes are reproduced through appropriate orifice coefficients [7].

Some oscillations are noticed in the computation of the total core mass flow rate but are linked to the accuracy or instabilities of the code.

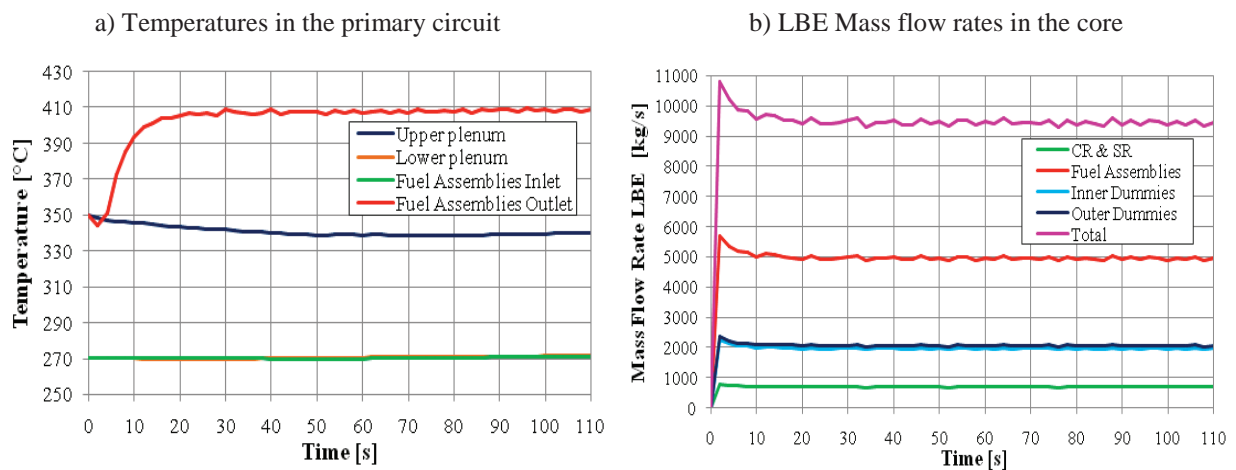


Figure 2.2: Trends of the steady-state calculation.

In Table 2.1, the main thermal-hydraulic computed parameters are compared with design values reported in [4] and [2]. Among the reference parameters the core thermal power was imposed as input of the model, the others were computed with SIMMER-IV. As steady-state calculation gave satisfactory results, the reached configuration was used as starting point for the computation of transients.

**Table 2.1: Thermal-hydraulic parameters: SIMMER-IV and design values.**

<b>PARAMETERS</b>	<b>UNIT</b>	<b>REFERENCE</b>	<b>SIMMER-IV j=50</b>
<b>Core thermal power</b>	MW	100	100
<b>Total mass flow rate</b>	kg/s	9440.8	9442
<b>FAs mass flow rate</b>	kg/s	4925.9	4949
<b>Core inlet LBE temperature</b>	°C	270	270
<b>Core outlet LBE temperature</b>	°C	410	408
<b>PHX inlet LBE temperature</b>	°C	350	347

### 3 FUEL DISPERSION ANALYSES

A parametric study on fuel dispersion with 3D model of MYRRHA reactor by SIMMER IV was performed in a previous work with the aim to evaluate the influence of some key parameters on the redistribution of the released fuel inside the primary circuit [7]. Results of this study highlighted the importance of stagnation zones for the accumulation of fuel particles. Then, the density difference between MOX and LBE, and the dimension of the released particles were found to have a significant influence on drag and buoyancy forces that affect the transport of fuel particles. The flow regime and the velocity pattern which stabilizes in the primary circuit are other key factors in the dispersion phenomena. Nevertheless, only analyses in forced circulation were achieved in [7] as the cover gas region was not simulated, so neither the level difference between hot and cold plena. The SIMMER-IV model with cover gas region was used to analyse the influence of natural circulation flow on the dispersion of the released fuel. For comparison purposes, the same model was used to perform two reference cases in forced circulation too. All the calculations with 3D model consider a fuel release equivalent to 1 fuel pin as reference and are discussed in Section 3.1.

Due to the large CPU time required for 3D simulations, the calculation time was in general limited to 500 seconds from the instant of fuel release. The rather short transient time is not enough to achieve steady-state conditions and quantify adequately the fuel particle behaviour in the medium and long term for the considered cases. For this reason, additional SIMMER-III calculations were performed in 2D geometry by enlarging the calculation time up to 1-2 hours. Parametric studies on the amount of fuel released, fuel density and fuel particles' diameter are performed in these 2D calculations, described in Section 3.2.

#### 3.1 SIMMER-IV fuel dispersion analyses

All the considered transients start after the steady-state condition at full power was reached. Each transient starts at  $t = 0$  s, when an amount of fuel particles equivalent to 1 fuel pin is released from a corner position in respect to the central In-Pile Section (IPS), as shown in Figure 3.1.

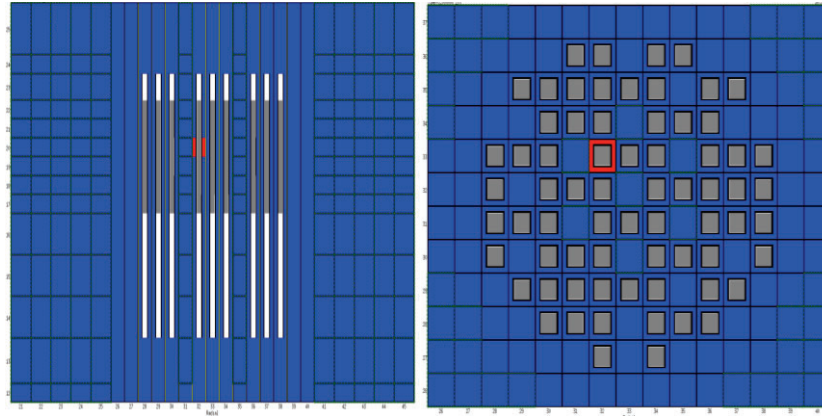


**Figure 3.1: Sketch of the position from whom the fuel is released.**

### 3.1.1 Fuel dispersion in natural circulation flow

In these simulations the particle release is supposed to be detected and the protection system intervenes. The loss of the pumping function occurs at  $t = 2$  s. The power level is set to decrease at 7% of the nominal level at  $t = 3$  s to simulate the control rod insertion and the residual decay power. Soon after the pump trip, the mass flow rate in the primary circuit is driven by the pressure differences. The LBE mass flow rate through the pumps, which is no longer driven by the suction head, decreases and even reverse. After that, it starts to oscillate up to stabilize in downward flow at the natural circulation mass flow rate. Likewise, the core mass flow rate starts to decrease up to reverse after the pump trip and oscillates before stabilizing again in upward flow.

Two cases, at fuel theoretical density and at 90% of theoretical density are treated. Fuel particle diameter is  $150\ \mu\text{m}$  for both cases.

For both the cases, fuel particles are transported by the LBE flow towards the upper part of the hot plenum during the first seconds of the transient. Nevertheless, the occurrence of a reversed flow through the primary pumps prevents the transportation of particles towards the PHXs. Then, the limited driving forces, which characterize the natural circulation, do not foster the diffusion of the fuel particles in the lower parts of the reactor. The behaviour in the long term depends on the fuel density, affecting the redistribution of the fuel particles.

Figure 3.2 and Figure 3.3 show the volume fraction of the cell occupied by the released fuel. In case of theoretical density, fuel particles tend to sink towards the lower part of the upper plenum and the core region. A low amount of fuel particles can be found in the diaphragm upper plate and in the lower sections. The highest amount of the released fuel remains in the central zone of the upper plenum ( $j=34-40$ ). Concentration at the LBE-gas interface ( $j=41-44$ ) is lower than in the sections below.

With fuel density at 90% of the theoretical value, the highest amount of particles tends to float and accumulates at the upper part of the plenum, near the LBE-gas interface ( $j=42-43$ ). This behaviour is linked to the value of the fuel density, which is lower than the LBE one when the porosity is at 10% (for further details see APPENDIX A). Fuel particle distribution is shown in Figure 3.3.

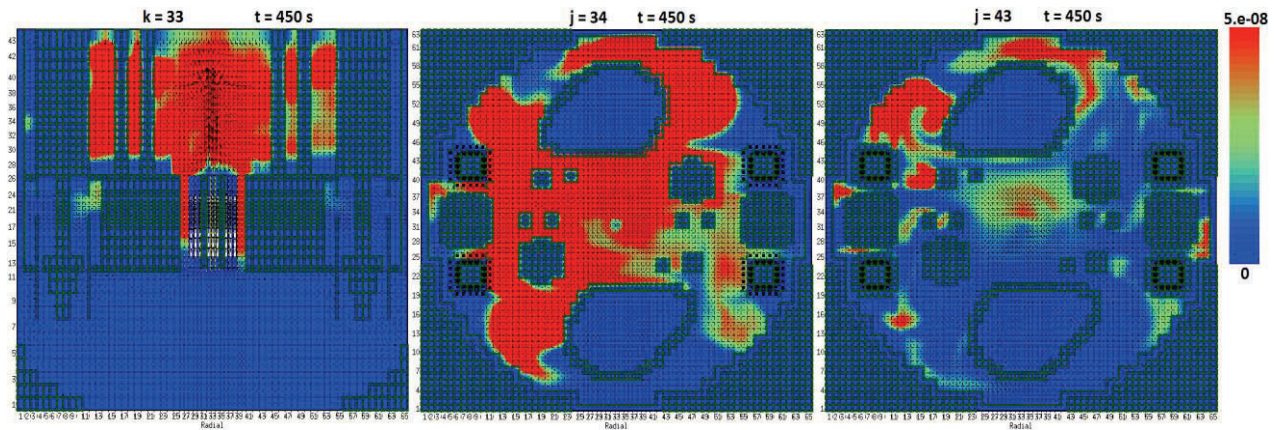


Figure 3.2: Volume fraction of fuel particles [-] in natural circulation, fuel at theoretical density.

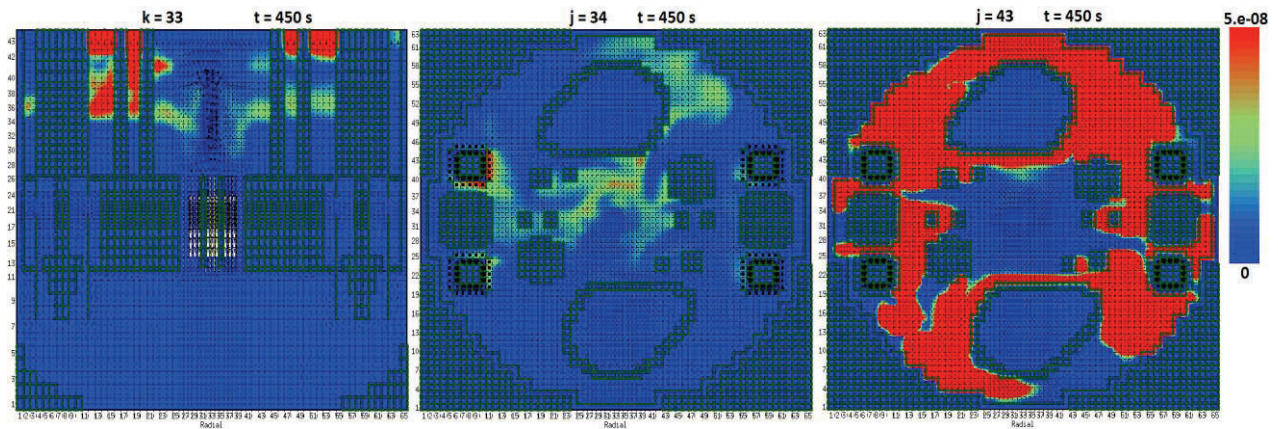


Figure 3.3: Volume fraction of fuel particles [-] in natural circulation, fuel at 90% of theoretical density.

### 3.1.2 Fuel dispersion in forced circulation flow

Two reference cases already analysed in a previous work [7] were chosen to be simulated also with the updated 3D model of the MYRRHA-FASTEF reactor and compared with the ones already performed. The aim was to evaluate if the differences between the models could affect the results on fuel particle dispersion. The boundary conditions set for these computations are both primary pumps and primary heat exchangers at nominal conditions and thermal power at 100% of nominal value too. This scenario simulates a fuel release accident without the intervention of the protection system. The two cases presented are both characterized by fuel at 95% of theoretical density but differ in the fuel particles diameter: 150  $\mu\text{m}$  and 800  $\mu\text{m}$ .

For both the considered cases the fuel particles are transported by the coolant and disperse quite homogeneously in the whole reactor, with no point of accumulation worth of note. In the case of fuel particles with diameter of 150  $\mu\text{m}$ , few accumulations of particles are noticeable in stagnation zones near the IVFHM (Figure 3.4). With fuel particles diameter equal to 800  $\mu\text{m}$ , the highest accumulation is detectable in the diaphragm upper plate, section j=27 (Figure 3.5). The higher particles diameter enhances the gravity forces, thus the sinking of the particles in the upper plenum.

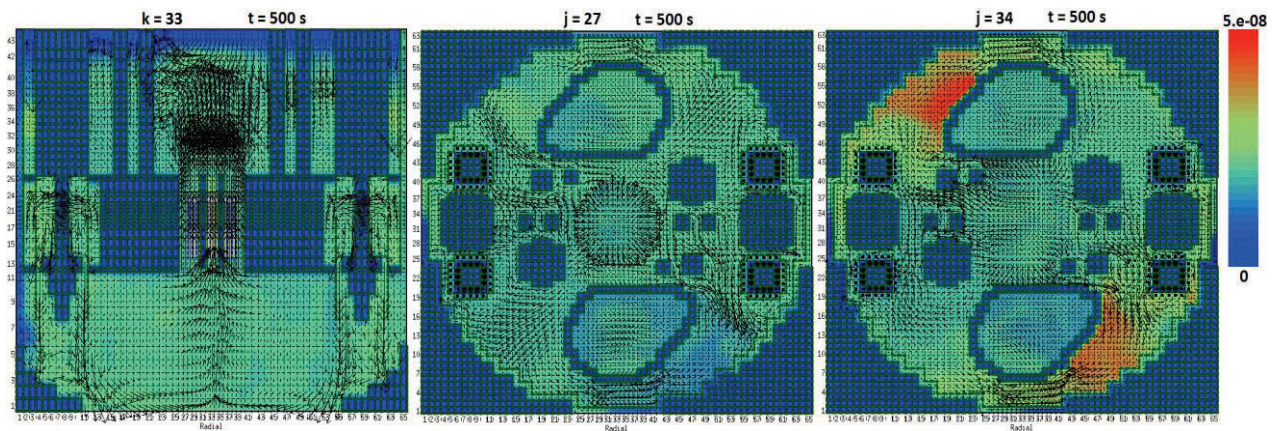


Figure 3.4: Volume fraction of fuel particles [-] in forced circulation, fuel particle  $\phi = 150\mu\text{m}$ .

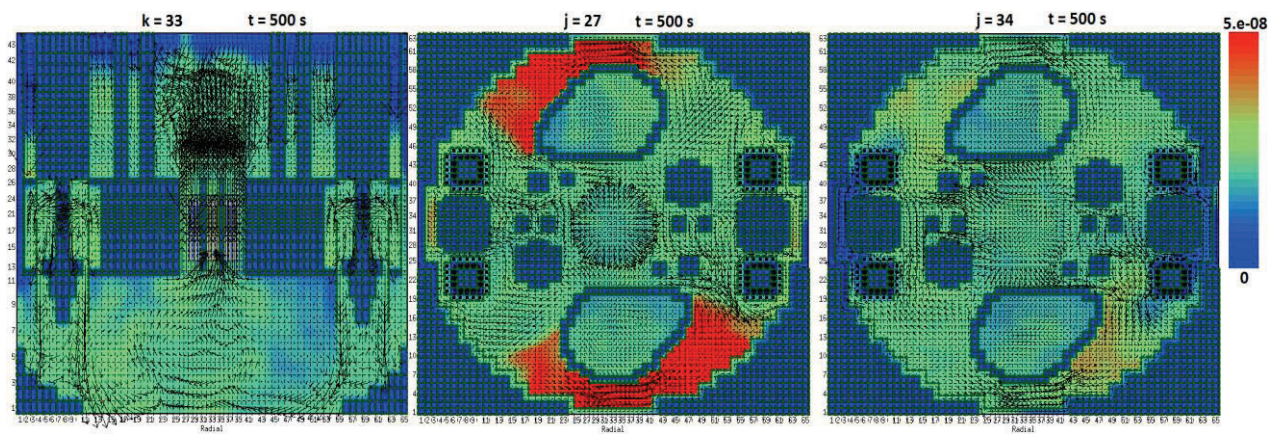


Figure 3.5: Volume fraction of fuel particles [-] in forced circulation, fuel particle  $\phi = 800\mu\text{m}$ .

A comparison with simulations performed with the previous model was attempted. It highlighted that using the model with cover gas region the dispersion of the fuel is more symmetric with respect to the older model, especially during the first part of the transient. The cause of this behaviour is attributable to the higher velocity field which establishes at the LBE-gas interface in the updated model. In particular, the horizontal velocity enhances the spreading of particles in whole horizontal sections, limiting the asymmetry in the redistribution. Nevertheless, the discrepancy between the two models becomes less important at the end of the simulation. The final distribution of the fuel inside the reactor is reported in Table 3.1. Using the new model, a higher part of the fuel is in the upper plenum and interface zones, instead in the old one it is found that more particles locate in the lower plenum. However, in the model with cover gas the volume of the upper plenum and interface is bigger than in the previous one, due to the free levels adjustment.

**Table 3.1: Percentage of the released fuel in the different macro-regions at the end of the transient.**

Fuel particle diameter	Reactor Model	Upper plenum + Interface [%]	Interface [%]	Diaphr. Upper Plate [%]	Lower Plenum [%]	Core [%]	PHX-Pump [%]	Annulus [%]	IVFHM [%]	Interface Annulus & IVFHM [%]
150 $\mu\text{m}$	old	25.94	0.09	1.75	48.15	0.79	8.22	5.00	10.15	-
150 $\mu\text{m}$	new	27.97	4.50	1.59	43.73	0.71	7.72	5.95	10.93	2.88
800 $\mu\text{m}$	old	23.56	0.00	2.51	49.82	0.78	8.09	6.39	10.11	-
800 $\mu\text{m}$	new	23.32	2.25	2.40	46.54	0.74	7.70	5.36	11.49	2.51

### 3.2 SIMMER-III calculations of fuel dispersion in the long term

The SIMMER-III model represents in 2D cylindrical geometry RZ (40x93 meshes) the main volumes of primary circuit and main components installed inside the vessel. The core is represented by several rings; the 4 PHX primary sides and 2 primary pump channels are represented by annular volumes with an equivalent cross flow area. The 2 fuel handling channels with cold LBE free level are represented by annular volumes on the outer part of the vessel. In the steady state calculation at nominal condition the LBE temperature at the core inlet is 270 °C and the total flow rate is 9440 kg/s following the design values. The main flow paths of the LBE coolant in the primary circuit are represented in 2D geometry. Nevertheless, the presence of stagnation zones observed in the 3D simulation of MYRRHA, mainly in the upper plenum, cannot be adequately represented in 2D geometry.

For the fuel dispersion analyses in the medium and long term, the cases with fuel porosity 5% and 10% and particle size 150  $\mu\text{m}$  and 800  $\mu\text{m}$  were considered. The same calculations were carried out with three different amounts of fuel release: the equivalent of 1 fuel pin, 1 fuel assembly and 60% of the core.

#### 3.2.1 Fuel release equivalent to 1 fuel pin

Results for the four cases with one fuel pin equivalent release are shown from Figure 3.6 to Figure 3.9. During the first part of the transient, the fuel particle concentration in the primary system does not depend significantly on fuel size and porosity of the fuel particles. By this time, the fuel particles move preferentially along the LBE flow pattern. From  $t = 500$  s some differences can already be observed in the particle distribution among the considered cases. In case of smaller particle size, the distribution is rather homogeneous as the drag forces induced by high coolant velocity predominate over the buoyancy forces. However, for 10% porosity, fuel particles are lighter than the coolant and tend to float. Some accumulation points are noticeable in the upper part of the PHX-pump compartment and just below the diaphragm lower plate. For bigger particle size, the buoyancy forces are more important and the accumulation process is accelerated. For 5% porosity, fuel particles are heavier than the coolant and thus start to preferentially accumulate on the bottom of the vessel. Conversely, for 10% porosity, the fuel particles are lighter than the coolant and thus start to accumulate in the upper part of the PHX-pump compartment and below the diaphragm lower plate.

The 2D results at  $t = 500$  s for the 5% porosity cases with different particle size can be compared to the 3D results presented in Section 3.1.2. Both 2D and 3D simulations predict rather homogeneous distribution of fuel particles in the primary volumes. However, the location of the main accumulation points is different, especially in case of bigger particles. These differences are mainly caused by the unavoidable simplifications introduced in the 2D geometry model of MYRRHA. In fact, the accumulation points of fuel particles are generally associated to more stagnant zones of coolant which can be realistically represented in 3D geometry only.

The fuel distribution in the primary circuit reaches an almost stabilized condition after  $t = 500$  s only in the case shown in Figure 3.6. In the other cases the fuel distribution continues to evolve afterwards. At

$t = 3600$  s, in the high porosity case with small diameter, fuel particles redistribution is less homogeneous and particles tend to accumulate towards the PHX-pump compartment and just below the diaphragm lower plate. Furthermore, fuel particles start to move up inside the annular external volumes with stagnant cold LBE. The accumulation at the cold LBE free surface is significant after 2 hours of transient (see Figure 3.7). With larger particle size the steady-state conditions are almost reached in about 1 hour. In the low porosity case (Figure 3.8) the fuel particles settle down on the lower plenum bottom. Conversely, in the high porosity case (Figure 3.9), due to buoyancy effects, the fuel particles accumulate in the more stagnant zones of the primary circuit: in the upper part of the PHX compartment, just below the diaphragm lower plate and at the cold LBE free surface.

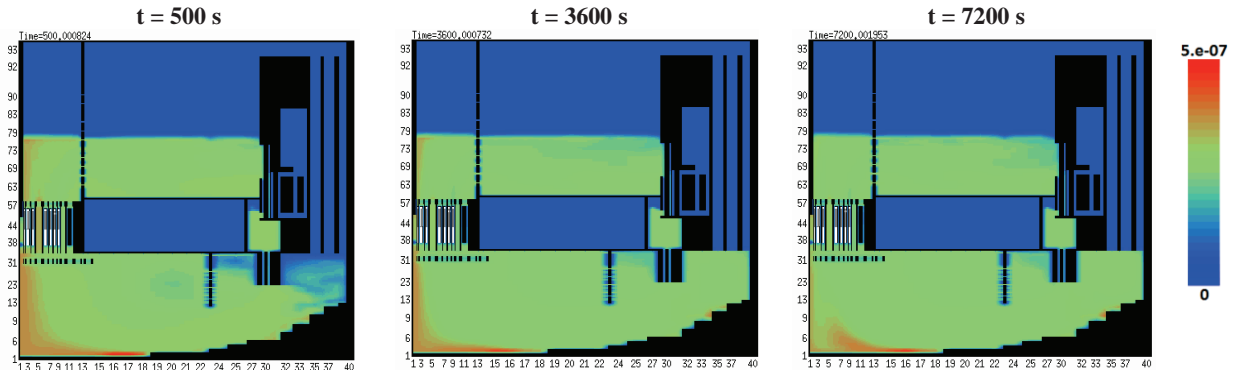


Figure 3.6: Volume fraction of fuel particles [-],  $\phi=150\mu\text{m}$ , fuel porosity 5%.

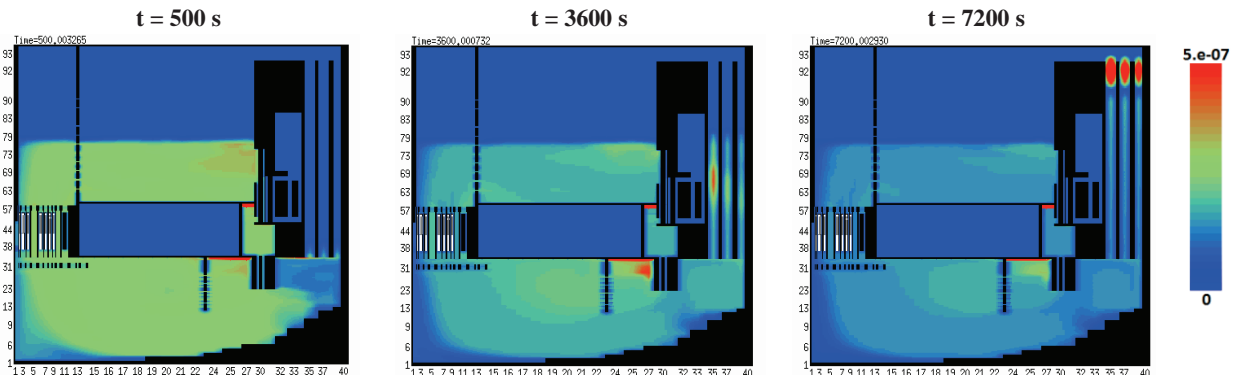


Figure 3.7: Volume fraction of fuel particles [-],  $\phi=150\mu\text{m}$ , fuel porosity 10%.

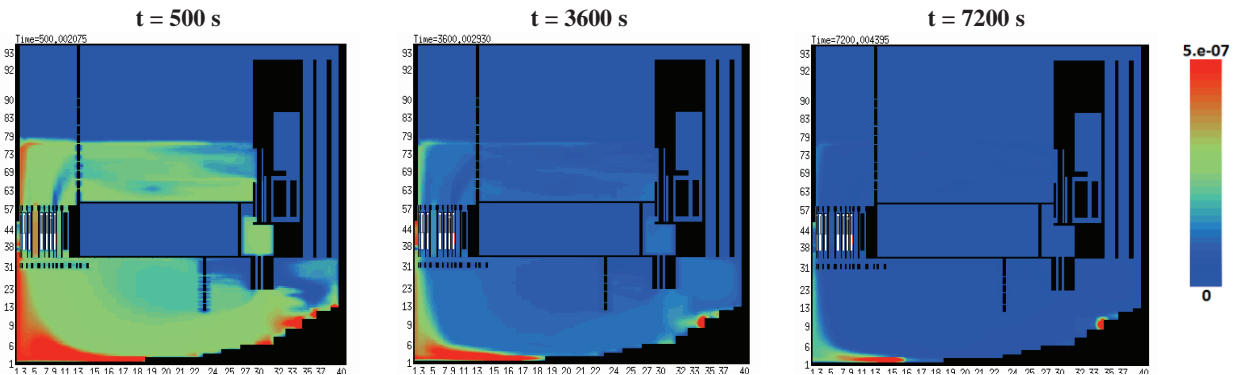


Figure 3.8: Volume fraction of fuel particles [-],  $\phi=800\mu\text{m}$ , fuel porosity 5%.

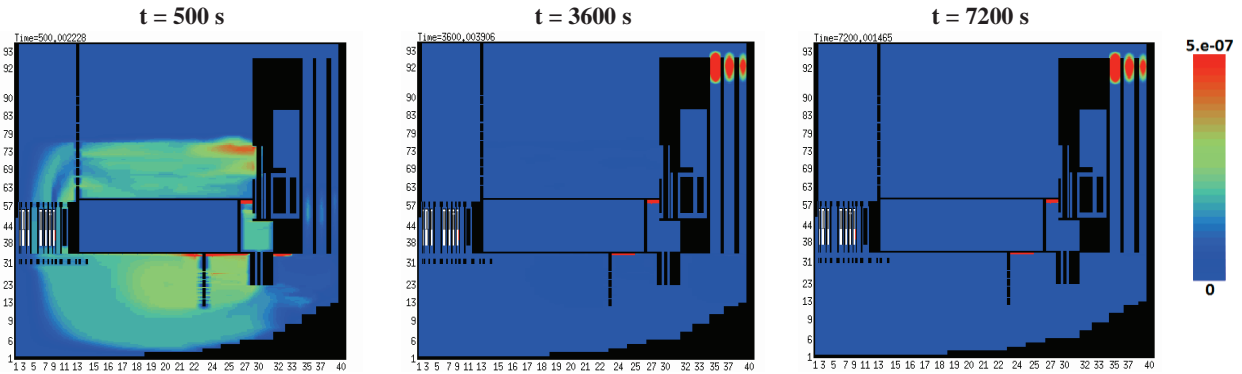


Figure 3.9: Volume fraction of fuel particles [-],  $\phi=800\mu\text{m}$ , fuel porosity 10%.

### 3.2.2 Fuel and clad particles dispersion at higher amount of released material.

For the cases with larger release, the clad particles are supposed to be released too. As for the smaller release, fuel is more or less homogeneously distributed in the primary circuit before  $t = 150$  s. However, the range for the volume fraction of fuel particles refers to a maximum of  $1.E-5$  for medium release (1 equivalent fuel assembly) and  $1.E-3$  for large release (60% of the core). For  $t > 500$  s the configuration of the fuel particles evolves in a similar way as already seen for the small fuel release cases. Figure 3.10 shows the cell volume fraction of fuel particles (ALPLK4) and steel particles (ALPLK5) after 1 hour of transient ( $t = 3600$  s) for the case of medium release. Released steel were considered with the same diameter of fuel particles.

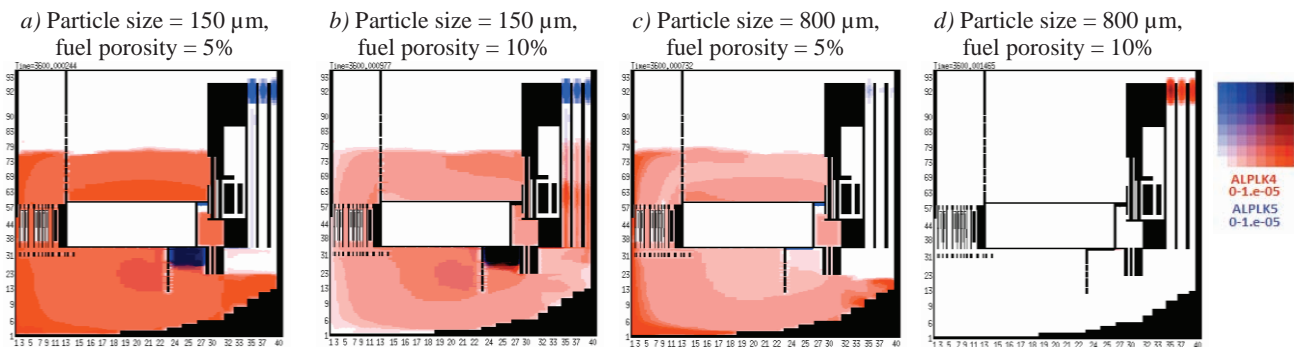


Figure 3.10: Volume fraction of fuel and steel particles [-] at  $t = 3600$  s.

Since the steel density is much lower than the LBE density, the steel particles tend to move toward the LBE free surface. However, because of the large drag forces in the upper plenum, no significant amount of steel particles remains at the LBE free levels surface in this region. The steel particles accumulate at the top of the PHX-pump compartment, just below the diaphragm lower plate and at the top of the external annular volumes.

The worst scenario for the risk of possible recriticality conditions seems the case with big particle size and high porosity (see Figure 3.9). Even in this case there are several accumulation zones that involve relatively large spreading volumes with rather low fuel concentration values. Therefore, the recriticality risk following a hypothetical severe accident with large fuel release seems very unlikely.

## 4 UNPROTECTED TRANSIENTS

In this section the analysis of the Unprotected Loss of Flow (ULOF) and the Unprotected Loss of Heat Sink (ULOHS) accidents is discussed. The aim is to investigate if the occurrence of these transients can cause a pin disruption and fuel release in the primary circuit. In SIMMER-IV simulations, only fluid-dynamic analysis was considered and coupling with neutronics is not taken into account. For this reason, the power trend that comprises reactivity feedbacks is imposed as input in our calculations. The trends were obtained from analogous calculations with RELAP5 code [8] and are shown in Figure 4.1. The simulations started after steady state conditions were reached, in order to have stabilized temperature and velocity fields in the primary circuit.

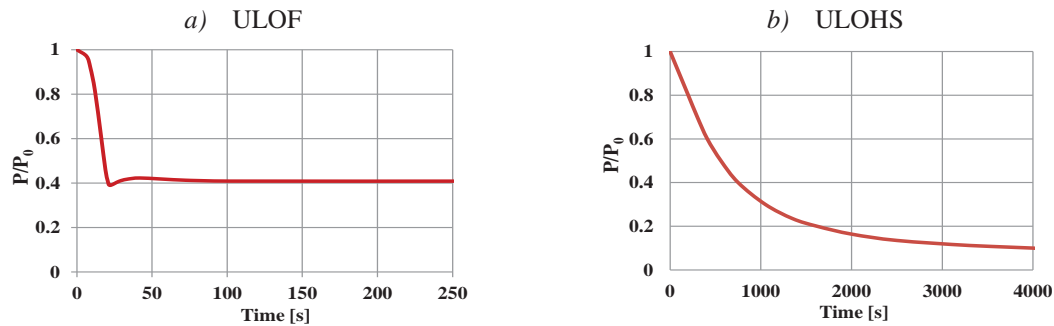
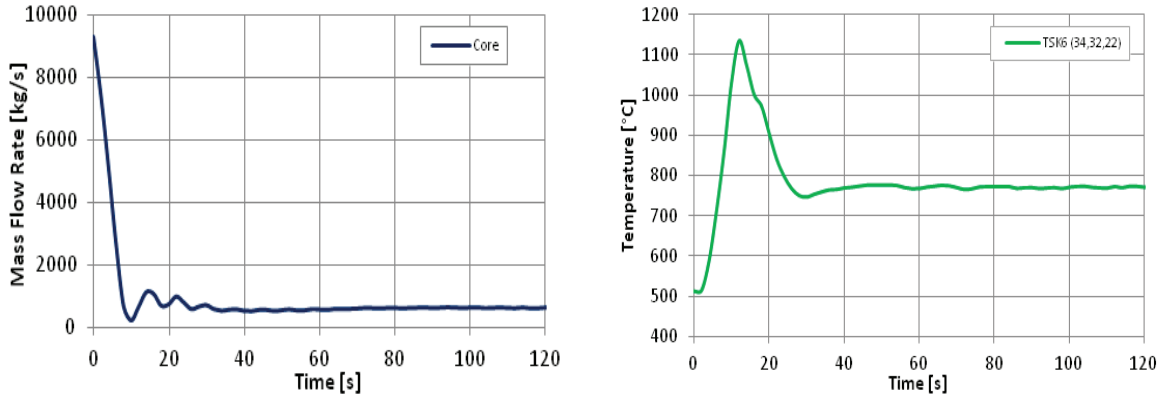


Figure 4.1: Power trend in input for unprotected transient calculations [6].

### 4.1 Unprotected Loss of Flow

For the simulation of the ULOF transient some assumptions are made. As said, the power level is imposed in the input of the calculation following the trend shown in Figure 4.1 *a*. The pumps stop working two seconds after the beginning of the simulation. During the transient, the heat removal through the secondary side is supposed to remain active.

After the pumps stop, the flow is driven by the equilibrium of the LBE free level between barrel, hot and cold plena. A reverse flow occurs at this time through the pumps up to about  $t = 8$  s. In absence of pumping head, the core mass flow rate decreases but, in this case, does not reverse. In fact, the power level is high enough to provide a driving force due to buoyancy sufficient to give positive mass flow rates in the core. As reported in Figure 4.2, the minimum in the core mass flow rate occurs at about  $t = 10$  s and leads to a degradation of the heat transfer. As the power level is high yet, the clad temperature starts to increase. The peak clad temperature occurs at about 12 s and reaches  $1135$  °C, but fuel pin degradation seems not to appear. After the increase in the core temperatures, the power decreases due to the reactivity feedbacks up to 40% of the nominal power. Then, the temperatures in the core decrease and, in the meanwhile, the natural circulation flow stabilizes in the primary circuit. At  $t = 70$  s, the core mass flow rate stabilizes at about 630 kg/s. A new steady state condition is reached in the core with a clad temperature of about  $770$  °C.



**Figure 4.2: Core mass flow rate and clad temperature in the hottest assembly during the ULOF accident.**

#### 4.2 Unprotected Loss of Heat Sink

The transient of Unprotected Loss of Heat Sink (ULOHS) is simulated with the SIMMER-IV code with some simplifying assumptions. The Loss of Heat Sink is simulated interrupting the heat transfer between the LBE and water through the primary heat exchangers, one second after the start of the simulation. Nevertheless, the pumps are assumed to remain active and so the forced circulation flow is provided during the transient. The resulting power level, imposed in the input of this calculation, is illustrated in Figure 4.1 *b*.

The loss of the PHXs function leads to a sharp increase in the LBE core inlet temperature, as shown in Figure 4.3. The increase in the core outlet temperature is less rapid as the power is decreasing. The clad temperature at the height of the Bottom of Active Fuel (BAF), for the fuel assembly with the highest power generation ( $i=34, k=32$ ), follows the progressive increase of the core inlet temperature. The peak clad temperature occurs at the Top of Active Fuel (TAF) of the same assembly. However, during the first 700 s, the clad temperature decreases due to reduction of the power generated. At the beginning of the transient, the core cooling is efficient due to the high thermal capacity of the LBE guaranteed by the forced circulation and the relative low temperatures. As the LBE temperature continues to increase, the heat transfer deteriorates and also the clad temperature at the TAF grows. In the first 2200 s of the simulation, clad temperatures do not go beyond 550 °C. Fuel pin degradation is unlikely to occur within the first hour of the transient.

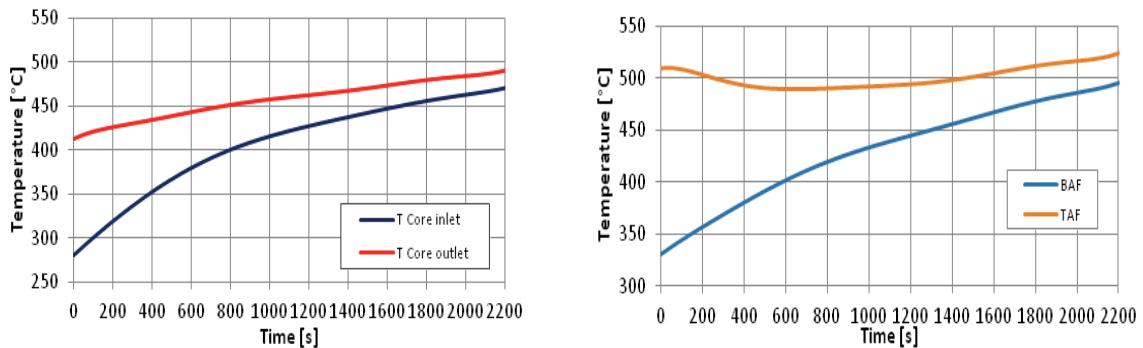


**Figure 4.3: LBE temperature (left) and clad temperature in the hottest fuel assembly (right), during ULOHS transient.**

## 5 CONCLUSIONS

A SIMMER-IV model of the MYRRHA reactor with a gas region above the primary LBE was set up to simulate properly the coolant level in the primary circuit. The suitability of the model was verified with a steady state calculation. Then, fuel dispersion analyses in natural circulation flow and for two reference cases in forced circulation were performed. In natural circulation flow, the occurrence of a reversed flow through the pumps after the trip and the establishment of a lower mass flow rate prevent the dispersion of the fuel particles in the primary circuit. The released fuel particles remain in the upper plenum and at the LBE-gas interface. Fuel dispersion in forced circulation with the new model confirmed the results of previous work [7]. Fuel particles dilute over the entire reactor with few accumulation points in both the considered cases. We noticed few differences in the dynamics of the dispersion at the beginning of the transient. Nevertheless, at the end of the transient, mass fractions of fuel particles in the different regions of the reactor are very comparable for the two models.

The 2D parametric simulations with SIMMER-III, performed to investigate the evolution of fuel concentration in the primary circuit in the longer term, confirmed that the fuel distribution is somewhat independent on the amount of fuel release. On the contrary, the sensitivity to particle size and porosity is important. The steady-state conditions are reached after 1 or 2 hour transient for all the cases. The phenomenon of particle accumulation is highlighted in case of big particle size and high porosity. With respect to the 3D simulation of MYRRHA, the 2D simulation introduces important distortion in the LBE velocity field, mainly in the upper plenum, so that the stagnant zones can differ from the 3D simulation. For this reason, the flow pattern in the primary circuit cannot be represented in a realistic way and the uncertainties on these 2D results are rather high.

The 3D model with the cover gas region allowed also the thermal-hydraulic calculations of ULOF and ULOHS transients. During the ULOF, the initial degradation of the heat transfer led to a sharp increase of the clad temperature. Afterwards, a new equilibrium at lower power and mass flow rate establishes and clad temperature stabilizes at a lower value. During the ULOHS, the lack of heat sink resulted in a progressive increase of the LBE and clad average temperatures. Nevertheless, for both the transients, no risk of fuel pin degradation is likely to occur for the time considered.

## NOMENCLATURE

2D	2-Dimensional
3D	3-Dimensional
CPU	Central Processing Unit
FA	Fuel Assembly
FASTEF	Fast Spectrum Transmutation Experimental Facility
FP	Framework Project
IVFHM	In Vessel Fuel Handling Machine
LBE	Lead Bismuth Eutectic
MYRRHA	Multi-purpose hYbrid Research Reactor for High-tech Applications
MOX	Mixed OXide
PHX	Primary Heat eXchanger
SA	Sub Assembly
SEARCH	Safe ExploitAtion Related CHemistry for HLM reactors
ULOF	Unprotected Loss of Flow
ULOHS	Unprotected Loss of Heat Sink

## ACKNOWLEDGMENTS

This work was performed in the framework of the SEARCH Project, funded by European Commission (FP7-EC).

## REFERENCES

1. Generation IV International Forum, "A Technology Roadmap for Generation IV Nuclear Energy System", December 2002.
2. R. Li, et al., "Studies of fuel dispersion after pin failure: Analysis of assumed blockage accidents for the MYRRHA-FASTEF critical core.", *Annals of Nuclear Energy*, **79**, pp. 31-42 (2015).
3. S. Buckingham, et al., "Simulation of fuel dispersion in the MYRRHA-FASTEF primary coolant with CFD and SIMMER-IV", *Proceedings of the SEARCH/MAXSIMA 2014 Workshop*, Karlsruhe, Germany, October 7-10, 2014.
4. H.A. Abderrahim, et al., "MYRRHA-A multi-purpose fast spectrum research reactor", *Energy Conversion and Management*, **63**, pp. 4-10 (2012).
5. Y. Tobita, et al., "The development of SIMMER-III, an Advanced Computer Program for LMFBR Safety Analysis and Its Application to Sodium Experiments", *Nuclear Technology*, **153**, (3), pp.245-255 (2006).
6. H. Yamano, et al., "Development of a three-dimensional CDA analysis code: SIMMER-IV and its first application to reactor case", *Nuc. Eng. Des.*, **238**, pp.66-73 (2008).
7. M.Eboli, et al., "Fuel dispersion and Flow Blockage Analyses for MYRRHA-FASTEF Reactor by SIMMER Code", *Proceedings of 2014 22<sup>nd</sup> International Conference on Nuclear Engineering (ICONE22)*, Prague, Czech Republic, July 7-11, 2014.
8. E. Bubelis, M. Schikorr, "FASTEF Safety Analysis – Critical Mode", Deliverable 2.3 (Part 1) of the Central Design Team (CDT) FP7 European Project (2012).

## APPENDIX A

The relative density between the fuel (MOX with 35% of plutonium) and the LBE is shown in Figure A. 1. Coolant density almost exclusively depends on temperature. Fuel density depends not only on temperature, but also on the degree of porosity. The porosity reduces fuel density with respect to the theoretical value. In turn, fuel porosity depends on fuel swelling under irradiation conditions and thus, porosity may increase from its initial value, 5%, to about 10% at the end of the irradiation cycle inside the reactor. On the contrary, the migration of the porosity at high temperature may lead to fuel compaction close to the theoretical density value.

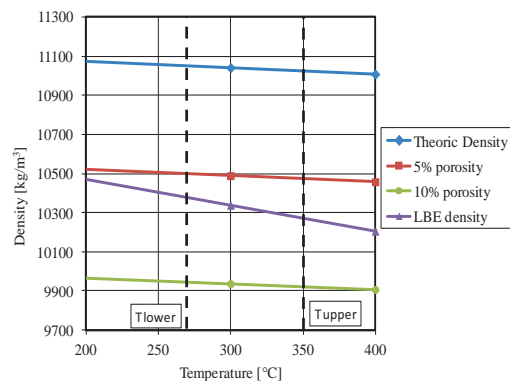


**Figure A. 1: Density versus temperature LBE and MOX at different porosity levels.**